A Photoemission Study of Solute−Solvent Interaction: Coadsorption of Na and H_2O on WSe_2 (0001)

Th. Mayer* and W. Jaegermann

Fachgebiet Oberflächenforschung, Fachbereich Materialwissenschaft, Technische Universität Darmstadt, Petersenstrasse 23, 64287 Darmstadt, Germany

Received: October 6, 1999; In Final Form: April 16, 2000

Semiconductor/electrolyte model interfaces are prepared in UHV by adsorbing and coadsorbing the electrolyte species Na and H_2O onto chemically inert van der Waals (0001) surfaces of WSe_2 at low temperatures (100K). The state of the adsorbed species is monitored by soft X-ray photoelectron spectroscopy (SXPS) and the surface potentials, i.e., band bending eV_{bb}, surface photovoltage SPV, electron affinity χ, and work function Φ by SXPS and ultraviolet photoelectron spectroscopy (UPS). H_2O coadsorbed to metallic Na clusters is dissociated and electron emission lines due to Na^+ and OH^- ions are observed. Coadsorption of Na to condensed ice layers preserves the H_2O molecules. The 3s electrons of the adsorbed Na atoms are transferred to the p-WSe_2 substrate as indicated by a depletion space charge layer on p-WSe_2. With increasing exposition to SX radiation, the 2p emission of the Na^+ ions is stepwise shifted to lower binding energy. We relate this successive shift to an increasing number of reorganized H_2O molecules from the adsorbate layer in its ice configuration to the hydration shell of Na^+.

1. Introduction

In this work we continue our approach toward an understanding of the semiconductor electrolyte interface on a molecular level via coadsorption of the electrolyte species onto defined crystal surfaces under ultrahigh vacuum conditions. General aspects of the application of UHV surface science techniques to the semiconductor/electrolyte interface are reviewed in.[1] The specific information which can be drawn from photoemisson experiments, especially with the use of synchrotron radiation, are related toward charge transfer across the interface, the value of interface dipoles, the chemical state of the interface and the density of occupied states (DOS) of the electrolyte.[1−3] The main purpose of this publication is to demonstrate that in coadsorption experiments using photoemission also the stepwise reorganization of solvation molecules and their effect on the DOS of an ionic electrolyte species, i.e., the reorganization energy λ may be measured. λ is one of the most important electrochemical parameters determining thermodynamic heats of solvation and thus the density of states distribution of the electrolyte and its redox potential.

Alkali metal cations and halogen anions solvated in free clusters have served as model systems for experimental[4] and theoretical[5,6] studies of solvation phenomena. There are a number of thermodynamic studies of stepwise solvation of ions which are reviewed in reference.[7] The reorganization energy was also determined by photo threshold measurements of ions in aqueous solutions.[8] There are also some applications of photoelectron spectroscopy to free clusters containing an ion solvated with a different number of solvent molecules.[9] Also coadsorption experiments of anions and cations with water on metal surfaces elucidating thermodynamic[10] and structural[11] aspects of the coadsorbate layer were performed. Specific changes in the development of the work function in the course of H_2O coadsorption to increasing amounts of preadsorbed Cs on Cu (110) were related to hydration.[12] The spectroscopic and structural results of a large number of alkali/water coadsorption experiments on metals were summarized in several reviews.[13,14] To our knowledge there are no observations of stepwise hydration in photoemission studies on surfaces published yet.

2. Experimental Section

The experiments were performed in a commercial UHV angle resolving spectrometer system (VG ADES 500) using synchrotron light at the BESSY TGM7 monochromator as excitation source. The overall resolution (fwhm) of the system as used was better than 0.3 eV. SXP spectra were excited with excitation energies for highest surface sensitivity. All emission lines are given as binding energy referred to the Fermi level E_B^F. The photoemission spectra are normalized to the excitation intensity given by the current of the refocusing exit mirror of the TGM7 monochromator. The base pressure of the analyzer chamber was below 10^{-10} mbar.

The WSe_2 crystals were prepared by chemical vapor transport and were p-type doped by Se excess with a density of about $10^{17}/cm^3$. The crystals were mounted with Ag epoxy to the sample holder which was in thermal contact to a liquid nitrogen bath. For flash annealing experiments the temperature could be raised by counter heating within 5 min from 100 to 140 K and recooled within 10 min to 100 K. The temperature was monitored with a thermocouple mounted to the sample holder. To separate the sample secondary electrons from the analyzer secondaries, a negative bias voltage of 5 V was applied. Na was deposited from SAES Getters alkali dispensers. The dosage is given in relative deposition times. The Na amount actually adsorbed is estimated in relation to the substrate core level photoemission intensity using theoretical cross sections σ.[15] H_2O was cleaned by several distillation cycles and adsorbed through a leak valve. The dosage is given in Langmuir (1 $L = 1.3 \times$

* Corresponding author. FAX: + 49 6151 166308. E-mail: mayerth@surface.tu-darmstadt.de.

10.1021/jp993563+ CCC: $19.00
Published on Web 06/03/2000

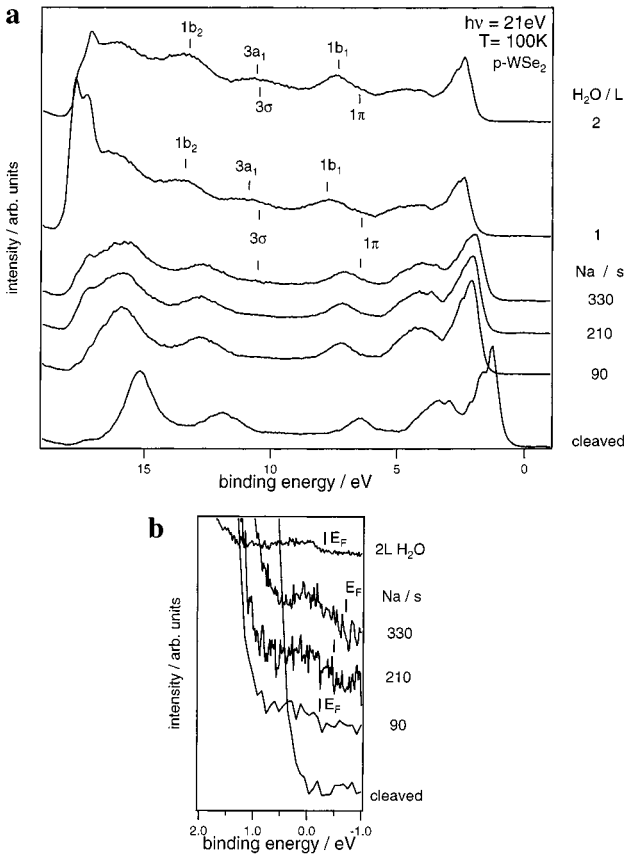

Figure 1. (a) Valence band spectra ($h\nu$ = 21 eV) in the course of adsorption of Na and coadsorption of H_2O onto p-WSe_2. Emission lines due to molecular orbitals of H_2O and OH^- are indicated. From bottom to top the spectra of the cleaved sample, the sample after 90, 210, and 330s Na adsorption and 1 *L* and 2 *L* H_2O coadsorption are displayed. After 330 s Na adsorption a formal coverage of approximately 0.1 is reached. (b) Close up of the Fermi level region of the spectra in Figure 1a. The Fermi edge of the adsorbed Na islands is shifted above the equilibrium Fermi level of the sample holder at 0.0 eV indicating a source induced photovoltage (SSPV). After H_2O coadsorption the SSPV is removed.

10^{-6} mbar s) determined by the uncorrected pressure rise in the deposition chamber. The samples were cleaved in a preparation chamber directly connected to the analyzer chamber where Na was deposited. H_2O was admitted in an additional adsorption chamber, which could be closed against the analyzer and Na dispenser while leaving the sample on the cooled sample holder.

3. Experimental Results

3.1. Coadsorption of H_2O onto Na preadsorbed p-WSe_2 (0001). The details of the interaction of Na adsorbed onto WSe_2 and other layered semiconductors under different experimental conditions have been discussed previously.[16,17] In accordance to the findings there at the given experimental conditions, i.e., low temperature of 100 K and UHV conditions, Na adsorption leads to the formation of a Schottky barrier on p-doped samples. The formation of the depletion layer is indicated by the shift of substrate emission lines to lower binding energy (see, e.g., the valence band spectra of Figure 1a and the W 4f core levels of Figure 4). The increased width of the valence band electron distribution curve (Figure 1a) indicates the drastic reduction of the electron affinity ($\Delta\chi = -0.9$ eV) adding up with the band bending ($eV_{bb} = -1.1$ eV) to a work function value close to bulk metal sodium (Φ WSe_2 / cleaved = 4.5 eV, Φ WSe_2 / Na

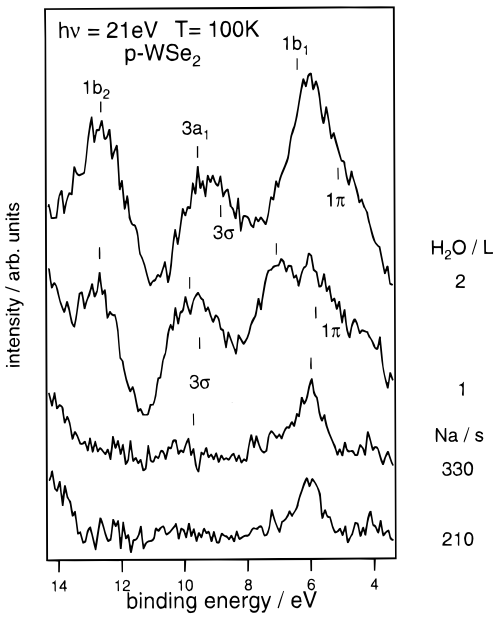

Figure 2. Difference spectra of the H_2O/Na coadsorption series in Figure 1. The spectrum of the freshly cleaved substrate is subtracted. The difference spectra after 210 and 330 s Na adsorption show some emission of the 3σ and 1π orbital of OH^- due to H_2O coadsorption via the residual gas. The intensities of these emissions increases drastically with deliberate H_2O coadsorption and aditional emissions due to the H_2O molecular orbitals $1b_2$, $3a_1$ and $1b_1$ appear with coadsorption of 1 and 2 *L* H_2O.

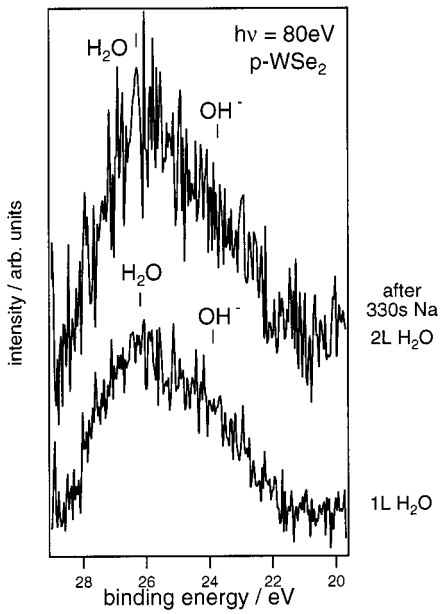

Figure 3. SXP-spectra ($h\nu$ = 80 eV) of the O 2s level for 1 and 2 *L* H_2O coadsorption to WSe_2 after 330 s Na adsorption. The two emission lines are addressed to H_2O and OH^-.

= 2.5 eV). A closeup of the Fermi level region (Figure 1b) shows the formation of the Na 3s conduction band. A source induced surface photovoltage (SSPV) shifts the Na 3s Fermi level above the reference Fermi level as measured on the Cu sample holder.[17−19] The formation of metallic Na is also indicated by the line shape of the Na 2p core emission (lower curve in Figure 4). Comparing the W 4f and Na 2p intensities a formal coverage of approximately 0.1 is reached ($\sigma_{W4f}/\sigma_{Na2p} = {}^1/_7$ at $h\nu$ = 80 eV). The metallicity at such low formal coverages indicates the strong clustering of the Na atoms on the chemically inert WSe_2 (0001) van der Waals surface.

TABLE 1: Surface Potentials and Binding Energy Values Measured for the System p-WSe_2/Na/H_2O: All Values Are Given in eV[a]

system	eV_{bb}	Φ	$\Delta\chi$	S-SPV	SPV	Na 2p E_b^F	Na^+ 2p E_b^F	H_2O $1b_1$ E_b^F	H_2O $1b_2$ E_b^F	H_2O 2s E_b^F	OH^- 1π E_b^F	OH^- 3σ E_b^F	OH^- 2σ E_b^F	H_2O $1b_1$ E_b^{vac}	H_2O $1b_2$ E_b^{vac}	H_2O 2s E_b^{vac}
p-WSe_2/Na	−1.1	2.5	−0.9	+0.4	+0.6	30.7										
p-WSe_2/Na/H_2O low coverage	−1.1	2.7	−0.7	+0.0	+0.5	30.7	31.7	8.1	13.9	26.1	6.3	9.9	24.1	10.8	16.6	28.8
p-WSe_2/Na/H_2O high coverage	−1.1	3.2	−0.1	+0.0	+0.5	30.7	31.7	7.1	13.6		6.0	9.4		10.3	16.8	
p-WSe_2/Na/H_2O after SXPS	−1.1	3.5	0.1	+0.0	+0.5		31.0	7.2	13.7	26.1	6.3	9.7	24.1	10.7	17.2	29.1

[a] eV_{bb}: and bending. Φ: work function. χ: electron affinity. SSPV: source induced SPV. SPV: surface photo voltage. E_b^F: binding energy related to the Fermi level. E_b^{vac}: binding energy related to the vacuum level.

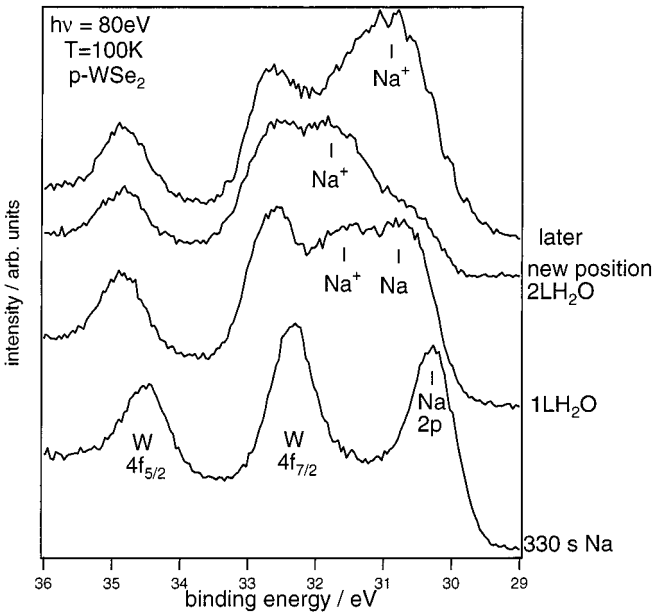

Figure 4. SXP-spectra ($h\nu$ = 80 eV) of the substrate W 4f and adsorbate Na 2p level after 330 s Na adsorption and 1 *L* H_2O coadsorption and 2 *L* H_2O coadsorption on a new position on the sample and after several minutes exposure to SX radiation. The two Na emission lines are addressed to metallic and ionic Na. The ionic component is shifted to lower binding energy after exposure to SX radiation.

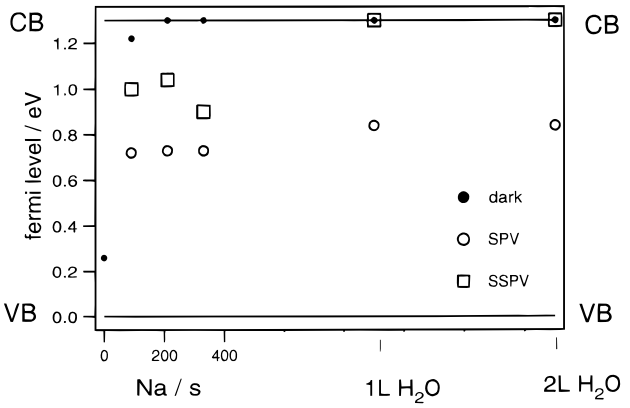

Figure 5. Position of the surface Fermi level in the course of Na adsorption and H_2O coadsorption in the dark and under illumination with the photoemission source (SSPV) and with additional white tungsten halogen bias light of 100 mW/cm^2 (SPV).

Coadsorption of H_2O leads to five additional emission lines in the valence band spectra of Figure 1a. The binding energy values are given in Table 1. Difference spectra (Figure 2) show that two of them were already present with low intensity before deliberate H_2O dosage. We address these two lines to the molecular orbitals 3σ and 1π of OH^- by comparison with e.g. dissociative H_2O adsorption on bulk alkali.[14] Their intensity increases drastically with H_2O dosage. The other three H_2O induced valence emission lines are clearly due to the H_2O molecular orbitals $1b_2$, $3a_1$ and $1b_1$.[20] The dissociation of a part of the coadsorbed H_2O molecules is also indicated by the two chemically shifted O 2s emissions displayed in Figure 3. As the pendant to the OH^- species a Na^+ component shows up on the high binding energy side of metallic Na (Figure 4). Surprisingly the binding energy of the 2p emission of Na^+ changes to lower values after exposure to the excitation source for several minutes during spectra accumulation. The overall intensity of the Na core emission is strongly enhanced with coadsorbed H_2O indicating the dissolution of the metallic Na islands. Interestingly, the SSPV is removed with coadsorbed H_2O and full band bending appears in the spectra. From a large number of experiments on differently doped samples we are able to relate substrate binding energies to the exact position of the surface Fermi level.[21] The position of the substrate surface Fermi level in the course of Na adsorption and H_2O coadsorption is displayed as SSPV in Figure 5. A correction of the SSPV by inspection of the measured Fermi level of the adsorbed Na clusters gives the surface Fermi level in thermodynamic equilibrium as also shown in Figure 5. Also included in Figure 5 is the surface quasi Fermi level position under irradiation with additional 100 mW/cm^2 tungsten halogen bias light. The difference to the equilibrium position (dark) indicates the photovoltage which can be obtained with the respective interface. The same value of band bending is found both for the semiconductor/metallic−Na−cluster interface and for the semiconductor/Na^+ + OH^- + H_2O interface. Thus, we follow the transformation of a semiconductor/metal Schottky barrier to a semiconductor/(model)electrolyte barrier. The surface potentials as the band bending eV_{bb}, the work function Φ, change of the electron affinity $\Delta\chi$, and the surface photovoltage SPV of the p-WSe_2/Na/H_2O interfaces and the binding energy values of the observed species referred to the Fermi level E_b^F and to vacuum E_b^{vac} are summarized in Table 1.

3.2. Coadsorption of Na onto H_2O Preadsorbed p-WSe_2 (0001). The details of the interaction of adsorbed H_2O on WSe_2 and other layered semiconductors have been reported previously.[22] Accordingly H_2O adsorbs molecularly at 100 K as indicated in the photoemission spectra by the fingerprint of the molecular valence orbitals $1b_2$, $3a_1$ and $1b_1$ in Figure 6 and a single emission line in the O 2s core level (Figure 7). H_2O induces electron transfer to the space charge layer on p-type layered chalcogenide (0001) surfaces. Because of band bending, the Fermi level moves all the way through the energy gap from a position close to the valence band maximum for the cleaved surface to a position close to the conduction band minimum at high H_2O coverages.[23] Due to low H_2O exposure in this experiment, only a small band bending shift of the substrate

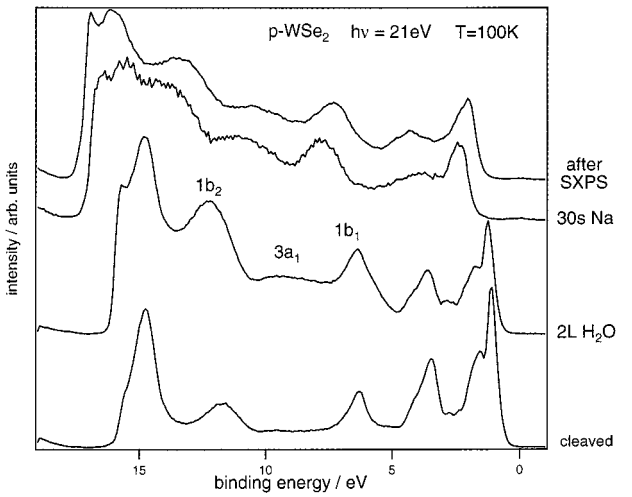

Figure 6. Valence band spectra ($h\nu = 21$ eV) in the course of H_2O adsorption and Na coadsorption onto p-WSe_2. The spectra of the cleaved sample and the sample exposed to 2 *L* H_2O and 30 s coadsorbed Na are displayed. Emission lines due to molecular orbitals of H_2O are indicated.

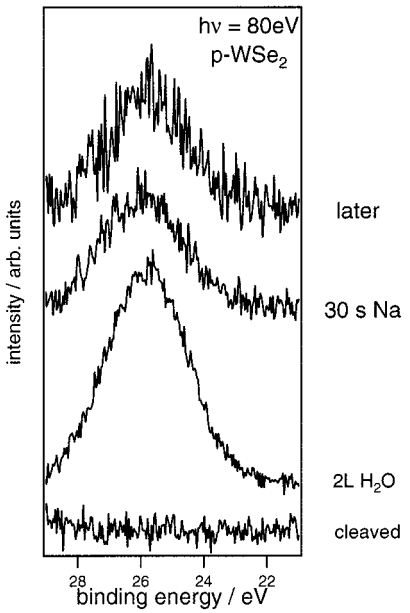

Figure 7. SXP-spectra ($h\nu = 80$ eV) of the O 2s level for Na coadsorption to H_2O on WSe_2. With coadsorbed Na still only a single emission line of H_2O is observed.

lines to lower binding energy is observed in the valence band spectra of Figure 6. Coadsorption of Na to the H_2O precovered p-WSe_2 is accompanied by a strong substrate level shift (see Figures 6 and 8) indicating band bending by electron transfer to the substrate. No additional emission lines are induced in the water valence band emissions (Figure 6). Also in the O 2s level (Figure 7) no indication of a second component is given with Na coadsorption. Thus, H_2O stays in its molecular adsorption state and is not dissociated in this case. The Na 2p emission (Figure 8) is found at very low binding energy as compared to metallic Na and therefore is assigned to ionic Na^+. Thus, the 3s electrons of the coadsorbed Na atoms are transferred to the substrate creating the space charge layer. The spectra shown in Figure 8 with coadsorbed Na are single scans taken one after the other with no parameter changed in between. The observed shift of the Na^+ 2p line from scan to scan is solely due to SXPS exposure. We observed similar shifts of the Na^+ 2p line induced by SX synchrotron radiation on different

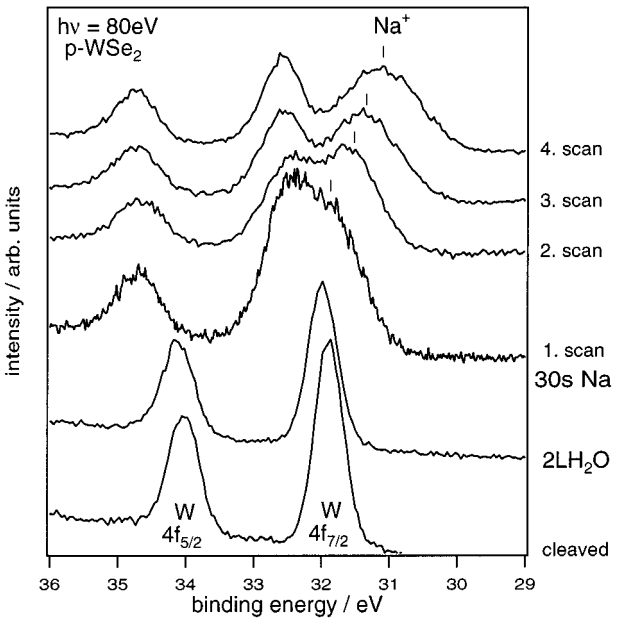

Figure 8. SXP-spectra ($h\nu = 80$ eV) of the substrate W 4f and coadsorbate Na 2p level in the course of H_2O adsorption and Na coadsorption. After Na coadsorption four scans were taken which are individually displayed. The Na binding energy indicates ionosorbed Na^+. The 2p binding energy is stepwise shifted to lower values due to exposure to SX radiation.

positions on the same sample as well as on different samples. A movement of the sample to a new SX unexposed position in close proximity to the exposed position gives the same Na 2p binding energy as was found originally at the beginning of the measurements displayed in Figure 8. The surface potentials of the p-WSe_2/H_2O/Na interface and the line positions of the observed species are summarized in Table 2.

We performed further coadsorption experiments on a different sample concentrating on the synchrotron light induced effect. Without taking any photoemission spectra after Na coadsorption, the first $h\nu = 80$ eV scan of the W 4f and Na 2p region (Figure 9) gives a binding energy of the Na^+ 2p line as low as 32.1 eV and a shift due to excitation by SX-radiation by -1.2 eV to 30.9 eV. The line positions versus scan number of Figure 8 and Figure 9 are displayed in Figure 10. A shift by the same amount may be induced by flash heating the H_2O/Na coadsorption system from 100 to 140 K and cooling the sample back to 100 K as documented by the spectra shown in Figure 11.

4. Discussion

The semiconducting WSe_2 substrate is stable under all experimental adsorption and coadsorption conditions we have applied in these experiments as no chemically shifted substrate emission lines were observed. The coadsorption of H_2O to metallic Na-clusters leads to the dissociation of a fraction of the coadsorbed water molecules. As the pendant to the detected OH^- species a Na^+ component appears on the high binding energy side of the metallic Na cluster component. Thus, the reaction

$$Na_{met} + H_2O \rightarrow Na^+ + OH^- + {}^1/_2\, H_2$$

takes place on the surface in accordance to bulk chemical expectations. With coadsorbed H_2O, the metallic Na clusters are evidently dissolved and the Na^+ ions are hydrated and more homogeneously dispersed on the surface as is indicated by an

TABLE 2: Surface Potentials and Binding Energy Values Measured for the System p-WSe_2/H_2O/Na: All Values Are Given in eV[a]

system	eV_{bb}	Φ	$\Delta\chi$	SPV	Na^+ 2p E_b^F	Na^+ 2p sample2 E_b^F	H_2O 1b_1 E_b^F	H_2O 1b_2 E_b^F	H_2O 2s E_b^F	H_2O 1b_1 E_b^{vac}	H_2O 1b_2 E_b^{vac}	H_2O 2s E_b^{vac}
p-WSe_2/H_2O	−0.2	4.8	−0.1				6.2	12.3	25.8	11.0	17.1	30.6
p-WSe_2/H_2O/Na	−1.1	3.8	−0.2		31.8	32.1	8.0	14.0	26.0	11.8	17.8	29.8
p-WSe_2/H_2O/Na after SXPS	−0.9	3.5	−0.7	+0.5	31.1	30.9	7.6	13.7	25.7	11.1	17.2	29.2

[a] eV_{bb}: band bending. Φ: work function. χ: electron affinity. SSPV: source induced SPV. SPV: surface photo voltage. E_b^F: binding energy related to the Fermi level. E_b^{vac}: binding energy related to the vacuum level.

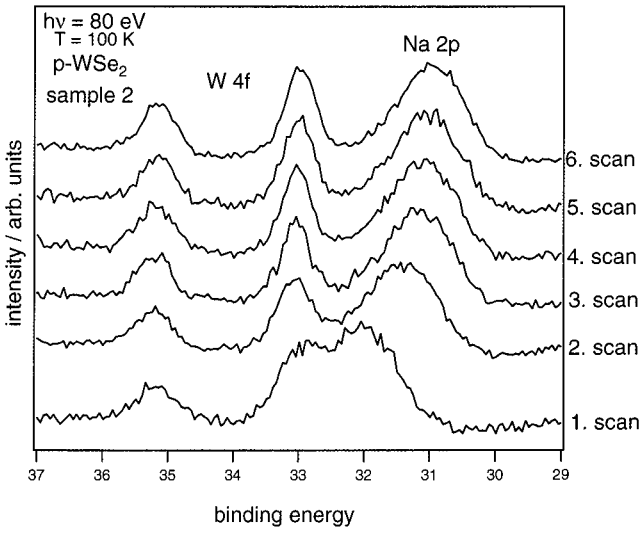

Figure 9. SXP-spectra ($h\nu$ = 80 eV) of the substrate W 4f and coadsorbate Na 2p level on sample 2. Six scans were taken after Na was coadsorbed to H_2O. No additional spectra were taken before the first scan or between the scans.

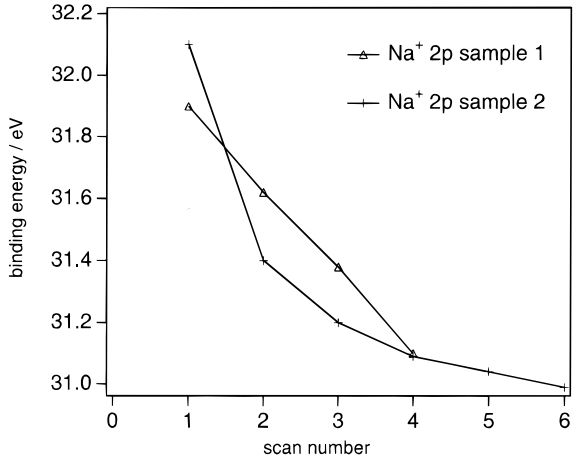

Figure 10. Line positions of the 2p level of coadsorbed Na in the experiments displayed in Figures 8 and 9 (sample 2).

increase of the relative Na emission intensities. Thus, we are following the transformation of a Schottky-barrier to a semiconductor/electrolyte model interface. While the Schottky-barrier height is equal in both situations the response to photoexcitation is different as indicated by the presence of SSPV for the metal islands and absence of SSPV after their dissolution (Figure 5). We can only speculate on the reasons for this behavior which follows from different generation and surface recombination rates in the two situations. Because of inhomogeneous surface potentials, with the metallic islands present, a reduced surface recombination of the generated electron−hole pairs is expected,[24,25] as compared to a higher recombination rate observed for homogeneous surface potentials as obtained after solvation.

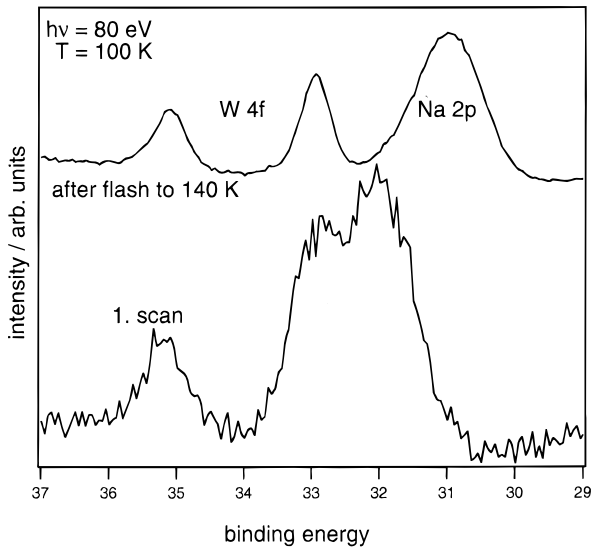

Figure 11. SXP−Spectra ($h\nu$ = 80 eV) of the substrate W 4f and the 2p level of coadsorbed Na at a new position of sample 2 before and after flashing to 140 K.

We observe three Na 2p emission line positions which we assign to metallic Na at E_b^F = 30.7 eV, unhydrated or partially hydrated Na^+ at E_b^F = 31.7 eV and after exposure to soft X-rays, hydrated Na^+ at E_b^F = 31.0 eV as tabulated in Table 1. The activation necessary for the shift of the Na^+ emission to lower binding energy is more clearly observed in the reversed coadsorption sequence and will be a main topic in the discussion later on. Similar binding energy shifts (−1 eV) of cationic potassium due to H_2O coadsorption have also been observed on Pt.[26] An ab initio cluster calculation led to the interpretation of increased electronic charge on the adsorbed K species due to H_2O coadsorption.[27] We are able to exclude this interpretation in our case since in contrast to metallic substrates the charge transfer between adsorbates and the substrate on semiconductors is monitored by changes of band bending. During H_2O coadsorption no change of band bending is observed.

Usually the H_2O monoadsorbate binding energies related to the Fermi level are found to be quite different on different metallic or semiconducting samples depending also on H_2O coverages while the ionization energies scatter in a narrow interval only. We have therefore assumed that the water induced dipole is mostly situated between the substrate surface and the water overlayer.[3] In the Na/H_2O coadsorption case we find the contrary behavior. The ionization energies of the water orbitals differ considerably in different adsorption steps while the binding energies are always similar. Therefore, in this case the position of the water induced dipole is situated at the adsorbate/vacuum interface. Also, the electron affinity is usually decreased with H_2O adsorption while it is increased for Na/H_2O coadsorption. This might be either directly due to the formation of OH^- which is known to increase the electron affinity.[20] Alternatively we would like to suggest that the H_2O molecules

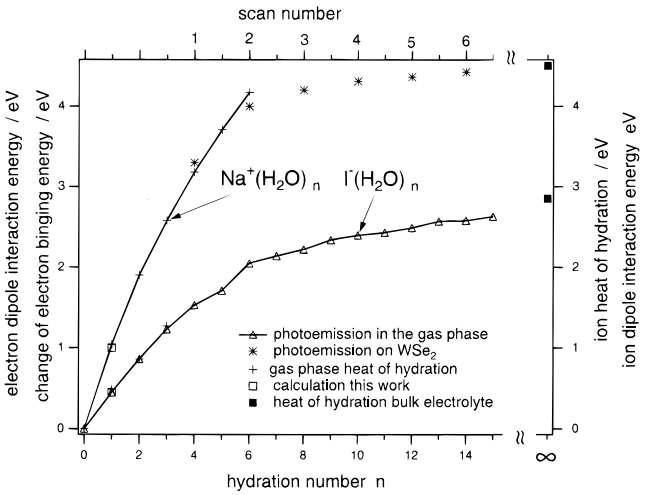

Figure 12. Comparison of I^- and Na^+ solvation data. Displayed are binding energy shifts as measured by photoemission experiments on gas-phase clusters[9] (triangles) and on WSe_2 surfaces (asterisks), thermodynamic heats of hydration[29,30] (plus signs), calculated values for hydration number one (open squares, see appendix) and single ion bulk hydration energies[31] (filled squares).

are reoriented in the field of Na^+ ions as discussed, e.g., for the Cu/Cs/H_2O system.[12,14,28]

By coadsorbing Na to H_2O on p-WSe_2 the absence of additional emission lines in the O 2s and water valence band states clearly indicates that no chemical reaction between the coadsorbates takes place. Since the line position at $E_b^F = 31.8$ and 32.1 eV (sample 2) and the line shape of the Na 2p level must be addressed to ionic Na^+, and since band bending is induced on the p-doped substrate, we conclude that the Na 3s electron is transferred to the substrate space charge layer. The binding energy of the H_2O orbitals are shifted considerably to higher binding energies right after Na coadsorption. We conclude that an electrical double layer is established by the Na^+ ions and the counter charge in the space charge region of the substrate with the water molecules sandwiched in between. This situation is typical for nonspecifically adsorbed alkali ions at the electrode/electrolyte interface.

The most striking feature of this coadsorption series is the stepwise shift of the Na^+ binding energy with the number of scans for obtaining SX-photoemission spectra. This effect as well as the thermal induced shift of Na^+ binding energy suggests a stepwise hydration of Na^+ by preadsorbed H_2O (solvation shift). For a more quantitative understanding of this effect, we would like to relate our measurements to thermodynamic gas-phase experiments on stepwise hydration of alkali cations and halide anions[29,30] as well as to gas-phase photoemission experiments of halogenide anions, where also a shift of binding energy with stepwise hydration was observed.[9] Unfortunately, the equivalent photoemission experiments on stepwise hydration of alkali ions are not available as yet. In Figure 12 we reproduce the negative value of the binding energy shifts measured for $I^-(H_2O)_n$.[9] A comparison to thermodynamic data[29] gives almost perfect agreement. Therefore, we assume that to a first approximation both the binding energy shift and the heat of hydration are mostly due to ion dipole interaction and that other effects[5,7,8] are small or cancel each other. As bench marks for the cluster experiments we use calculated values (see appendix) for the first hydration step on the left and heats of hydration of single ions in bulk electrolyte[31] which should be approached by the gas phase and surface cluster studies on the right side of Figure 12. In Table 3 the calculated values are compared to

TABLE 3: Calculated and Experimental Values of the Dipole Potential $|e_o\Psi|$, Heat of Hydration ΔH of a Single H_2O Molecule and Bulk Water and Photoemission Binding Energy Shifts ΔE_B:All Values Are Given in eV

	$\lvert e_o\Psi\rvert$[a]	ΔH[b,c] single	ΔE_B[d] single	ΔH[e] bulk	ΔE_B[d] $(H_2O)_{15}$
I^-	0.44	0.44	0.45	2.8	2.63
Na^+	0.94	1.04		4.4	

[a] See Appendix. [b,c] References 28 and 29. [d] Reference 9. [e] Reference 30.

measured heats of hydration of a single water molecule[29,30] and for I^- to the experimental binding energy shift in photoemission.[9] Also listed are the hydration values of the respective ions in bulk water which may be compared to the binding energy shift measured on the $I^-(H_2O)_{15}$ cluster. Again we find good agreement in the I^- case.

This finding is remarkable in itself. It states that the heat of hydration of an ion can be monitored with photoemission by the solvation shift of its electrons. While the heat of hydration is considered as a measure of the interaction of the solvent dipoles with the net charge of an ion it is actually the sum of the interaction of the solvent dipoles with the individual electrons and protons of the ion. With photoelectron emission, the interaction of the solvent dipoles with an individual electron is measured. Since the charge of the ion as well as the charge of the electron is one elementary unit, the solvation binding energy shift and the heat of hydration are of equal value when the most simple point charge−point dipole model is applied. A thorough experimental test of this theory would be the measurement of the heats of stepwise hydration and solvation shifts on a doubly charged ion. Here the two observables should differ by a factor of 2. It should be noted that we have interpreted our results as initial state effects namely the change of the electron binding energy of the ground state by the solvation shell. In principle also the change of the screening of the photoemission hole—the final state effect—may lead to shifts of the emission lines as, for example, those measured for clusters with increasing size (see, e.g., ref 32). However, because our experiments are performed on substrate surfaces, we believe that changes in screening play a minor role.

Although for the Na^+ case the data do not quite as well fit together as in the I^- case, we think the comparison of the data drawn from such diverse sources is still instructive. Albeit not knowing the hydration number in our surface experiments we tentatively fit our measured binding energy shifts versus scan number from the spectra of Figure 10 to the gas-phase cluster experiments. This comparison allows a rough correlation of scan number and hydration number.

Although the hydration of Na^+ may also be activated thermally (Figure 11) we propose an indirect photoactivation process for the stepwise photoemission source induced hydration. Two arguments lead to this assumption. First, we never observed photoinduced desorption of H_2O which already occurs at approximately 150 K under our experimental conditions. Second, in close proximity to the photoexcitation spot, no hydration occurred while thermal effects due to the source should be less local. The observed indirect photoinduced process would be in analogy to the recently discovered photoinduced transformation of amorphous to crystalline ice films on graphite via secondary photoelectrons from the substrate.[33]

We are led to the following picture of the coadsorption of Na to p-WSe_2 /H_2O (Figure 13a): As the Na atom approaches the surface, it transfers its 3s electron to the substrate and is ionosorbed on top of the preadsorbed ice layer. Thus, it coordinates to three to four water molecules without reorienting

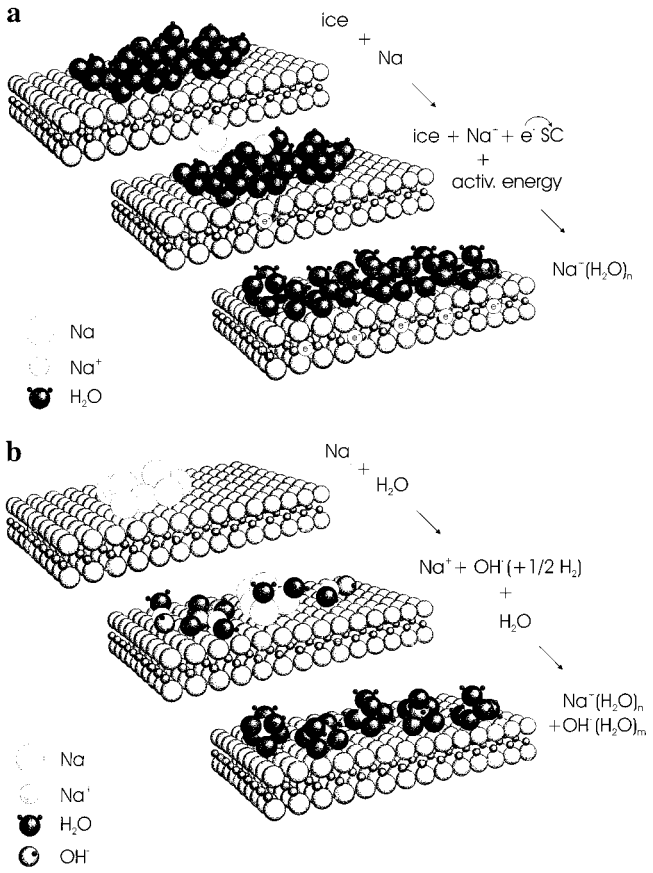

Figure 13. (a) Visualization of the experimental results of the coadsorption of Na to p-WSe_2/H_2O: Initially a H_2O ice layer is adsorbed. Coadsorption of Na leads to a charge transfer of the Na 3s valence electron to the p-WSe_2 substrate. The Na^+ ion formed is subsequently hydrated by excess H_2O molecules in an activated process. (b) Visualization of the experimental results of the coadsorption of H_2O to p-WSe_2/Na: Initially Na is adsorbed as metallic Na clusters. Coadsorption of H_2O leads to the formation of Na^+ and OH^- The Na^+ ions are hydrated by excess H_2O molecules in an activated process. We tentatively draw the OH^- ions also hydrated.

these molecules out of the given ice layer. The reorganization of the water molecules from the given ice coordination to an hydration geometry around the Na^+ ion is subsequently induced either thermally or nonthermally via an indirect photoactivated process. The H_2O molecules are not dissociated in this coadsorption sequence.

In the case of coadsorption of H_2O to p-WSe_2/Na we can visualize our experimental results in the following picture (Figure 13b): The originally adsorbed metallic Na clusters are dissolved by the coadsorbed H_2O forming Na^+ and OH^- ions. The Na^+ ions are again bound in an hydration shell by additionally coadsorbed H_2O molecules giving rise to similar spectral features as in the above-discussed case. Although we observe little or no shift of the OH^- ions to higher binding energy in the presented experiments we tentatively draw a solvation shell around the OH^- anions in Figure 13b. In summary the final binding energy measured for Na^+ in both coadsorption sequences is nearly identical and evidently is strongly influenced by solute/solvent interactions.

5. Summary

While the coadsorption of H_2O to metallic Na clusters on p-WSe_2 is accompanied by the dissociation of the water molecule, no such reaction occurs in the reverse adsorption sequence. The difference in reactivity may be related to the fact that dissociative adsorption of H_2O demands bonding sites for both hydroxyl and hydrogen atom which evidently is only realized on the Na clusters. In both adsorption sequences Na is finally adsorbed as an ion either by the reaction with H_2O or by charge transfer to the substrate. The binding energies of the Na^+ states are shifted from an initially high binding energy to lower values induced by the exposure to SX photons or thermally. We relate these activated shifts to an increasing number of water molecules forming an hydration shell around the ion and call it solvation binding energy shift. The obtained data are compared to photoemission studies of stepwise solvation experiments of halide anions in the gas phase and to heats of stepwise hydration which show surprisingly good agreement among one another. This comparison allows us to roughly relate exposure time (scan number) to hydration number. The presented results indicate that the investigation of model electrolytes prepared by the coadsorption of electrolyte species gives valuable information also on the solute/solvent interaction (solvation). We plan to extend our approach for a more quantitative investigation of solvation using SXPS studies in a more controlled (stepwise) adsorption of the respective species applying thermal activation of solvation after each H_2O adsorption step. Thus, the measured binding energy shifts may be experimentally related to the hydration number and geometry.

Acknowledgment. This work was suppoerted by a grant of the BMBF. Experimental help of J.Lehmann and the support of the BESSY staff is gratefully acknowledged.

6. Appendix

Photoemission binding energy shifts induced by hydration. The ion−dipole interaction energy U is equal to the charge $z_i e_o$ of the ion times the potential $\Psi_{(r,\theta)}$ due to the dipole at the site of the ion: $U = z_i e_o \Psi_{(r,\theta)}$.$\Psi_{(r,\theta)}$ of a dipole being placed at a distance r from the ion oriented at an angle θ may be calculated in the dipole approximation as

$$\Psi_{(r,\theta)} = \frac{1}{4\pi\epsilon_o\epsilon_r}.\frac{\vec{\mu}\cdot\vec{r}}{\vec{r}^3} = \frac{1}{4\pi\epsilon_o\epsilon_r}.\frac{\mu\cos\theta}{r^2}$$

In the gas-phase we may assume the dielectric constant of vacuum $\epsilon_r = 1$. For a single water molecule, we assume $\theta = 0$ and a dipole moment $\mu = 1.85$ D. As the distance r we take the sum of the water molecule radius $r_{H_2O} = 0.14$ nm and the ion radius. The radii are $r_{I^-} = 0.216$ nm and $r_{Na^+} = 0.102$ nm.[34,35] The calculated $\Psi_{(r,\theta)}$ values are listed in Table 3.

References and Notes

(1) Jaegermann, W. In *Modern Aspects of Electrochemistry*; White, R. E., Ed.; Plenum Press: New York, 1996; Vol 30, p 1.
(2) Jaegermann, W.; Mayer, Th. *Surf. Sci*. **1995**, *335*, 343.
(3) Mayer, Th.; Jaegermann, W. In *Synchrotron Techniques in Interfacial Electrochemistry*; NATO ASI C 432; Melendres, C. A., Tadjeddine, A., Eds.; Kluwer: Dordrecht, 1994; 451.
(4) Kebarle, P. *Annu. Rev. Phys. Chem*. **1977**, *28*, 445.
(5) Kistenmacher, H.; Popkie, H.; Clementi, E. *J. Comput. Phys*. **1974**, *61*, 799.
(6) Bekmuratova, E. M.; Pozharov, S. L.; Khabibullaev, P. K. *Russ. J. Phys. Chem*. **1983**, *57*, 1171.
(7) Castleman, A. W., Jr.; Keesee, R.; G. *Chem. Rev*. **1986**, *86*, 589.
(8) Delahay, P. *Acc. Chem. Res.* **1982**, *15*, 40.
(9) Markovich, G.; Giniger, R.; Levin, M.; Cheshnovsky, O. *J. Chem. Phys.* **1991**, *95*, 9416.
(10) Bange, K.; Döhl, R.; Grieder, D. E.; Sass, J. *Vacuum* **1983**, *33*, 757.
(11) Bange, K.; Madey, T. E.; Sass, J. *Surf. Sci*. **1985**, *162*, 252.

(12) Sass, J.; Lackey, D.; Schott, J.; Straehler, B. *Surf. Sci*. **1991**, *247*, 239.
(13) Bonzel, H. P. *Physics and Chemistry of Alkali Metal Adsorption*; Elsevier: Amsterdam, 1989.
(14) Bonzel, H. P. *Surf. Sci. Rep*. **1987**, *8*, 43.
(15) Yeh, J. J.; Lindau, I. *At. Data Nucl. Data Tables* **1985**, *32*, 1.
(16) Schellenberger, A.; Schlaf, R.; Mayer, Th.; Holub-Krappe, E.; Pettenkofer, C.; Jaegermann, W. *Surf. Sci. Lett*. **1991**, *241*, L25.
(17) Schellenberger, A.; Schlaf, R.; Pettenkofer, C.; Jaegermann, W. *Phys. Rev. B* **1992**, *45*, 3538.
(18) Horn, K.; Alonso, M.; Cimino, R. *Appl. Surf. Sci*. **1992**, *264*, 65.
(19) Hecht, M. H. *Phys. Rev. B* **1990**, *41*, 7918.
(20) Thiel, P. A.; Madey, P. E. *Surf. Sci. Rep*. **1987**, *7*, 211.
(21) Mayer, Th.; Pettenkofer, C.; Jaegermann, W. *J. Phys. Chem*. **1996**, *100*, 16966.
(22) Mayer, Th.; Klein, A.; Lang, O.; Pettenkofer, C. *Surf. Sci*. **1992**, *269/270*, 621.
(23) Mayer, Th. *Doktorarbeit* 1993.
(24) Schlaf, R.; Sehnert, H.; Pettenkofer, C.; Jaegermann, W. *Mater. Res. Soc. Symp. Proc*. **1991**, *221*, 137.
(25) Schlaf, R.; Klein, A.; Pettenkofer, C.; Jaegermann, W. *Phys. Rev. B* **1993**, *48*, 14242.
(26) Bonzel, H. P.; Pirug, G. *Chem. Phys. Lett*. **1985**, *116*, 133.
(27) Bonzel, H. P.; Pirug, G. *Phys. Rev. Lett*. **1987**, *58*, 2138.
(28) Doering, D. L.; Semancik, S.; Madey, T. E. *Surf. Sci*. **1983**, *133*, 49.
(29) Arshadi, M.; Yamdagni, R.; Kebarle, P. *J. Phys. Chem*. **1970**, *74*, 1475.
(30) Dzidic, I.; Kebarle, P. J. *Phys. Chem*. **1970**, *74*, 1467.
(31) Bockris, J. O. M.; Reddy, A. K. N. *Modern Electrochemistry*, Plenum Press: New York, 1998.
(32) Wertheim, G. K. *Phys. Rev. B* **1989**, 33.
(33) Chakarov, D.; Kasemo, B. *Phys. Rev. Lett*. **1998**, *81*, 5181.
(34) Lide, D. R. *Handbook of Chemistry and Physics*, CRS: Boca Raton, 1993.
(35) Israelachivili, J. N. *Intermolecular and Surface Forces*; Academic: New York, 1992.